

Rethinking the Nature of Light: The Binary Photon and the Point Spread Function

Margaret Lovier^{1,2}, Mamta Srivastava³ and Randy Wayne^{1*}

¹Laboratory of Natural Philosophy, Plant Biology Section, School of Integrative Plant Science, Cornell University, Ithaca, New York 14853, USA and ³Plant Cell Imaging Center, Boyce Thompson Institute, Cornell University, Ithaca, NY 14853

Abstract

Images of sub-resolution fluorescent microspheres taken with a laser scanning confocal microscope do not appear as spheres but as prolate ellipsoids relative to the optical axis of a microscope. The full width at half maximum (FWHM) intensity of the major axis of the ellipsoid is greater than the FWHM intensity of the minor axis of the ellipsoid by $\pi \frac{n}{NA}$, where π is a factor that depends on the geometry of the binary photon and $\frac{n}{NA}$ is a factor that depends on the geometry of the optical system. The standard equations of confocal microscopy are inadequate describers and predictors of these results. However, the lateral and axial resolution equations that are based on Rayleigh's criterion and derived from the Kirchhoff diffraction equation whose assumptions are met by the binary photon are not only better describers and predictors but also explainers of the quantitative spatial aspects of the images. The accuracy of the equations that are based on the model of the binary photon in predicting the FWHM of the images of the fluorescent microspheres support the claim that binary photons, which exhibit wave-particle duality as a consequence of the motions of two oppositely-charged particles that give rise to wave-like electromagnetic fields may be the fundamental and irreducible component of light.

You can observe a lot by just watching.—Yogi Berra

²We thank the School of Integrative Plant Science for the grant awarded to Margaret Lovier that made these experiments possible.
^{*}email: rowl@cornell.edu

1. Introduction

According to geometrical optics, the image formed by a perfect aberration-free lens is a point-by-point representation of the object [1]. In theory, obtaining a point-by-point image of an object requires the photon to be a symmetrical, zero-dimensional, mathematical point. Otherwise the photons themselves would blur the boundaries of each point. High-resolution confocal laser scanning microscopy allows one to test whether the photon satisfies the assumptions of geometrical optics and is a zero-dimensional symmetrical mathematical point or whether the photon is an asymmetrical and extended entity.

The inflation of object points into image volumes, also known as three-dimensional point spread functions [PSF; 2,3], cannot be explained in terms of quantum mechanical photons but can be explained by diffraction that results from the limitations of the optical system and the wave nature of light. The Kirchhoff diffraction equation based on wave theory can be successfully employed to describe observations using confocal microscopy that geometrical points in the object appear as asymmetrical prolate spheroids in the image. However, according to Henri Poincaré and Arnold Sommerfeld, the assumptions upon which the Kirchhoff diffraction equation are based, are not fulfilled by light that is modeled in real space as standard Maxwellian electromagnetic plane waves. Thus unless one uses imaginary space, there is an unresolved contradiction in using both the Kirchhoff diffraction equation and the Maxwellian electromagnetic wave description of light. The contradiction can be avoided by using the model of the binary photon whose electric and magnetic fields are out-of-phase by a quarter of a wavelength, and thus fulfills the assumptions of the Kirchhoff diffraction equation in real space [4].

The inflation of object points into image volumes can be observed and measured in a confocal microscope using sub-resolution fluorescent microspheres as objects [5]. The sub-resolution microspheres act as point sources of light and each point of light is spread into an Airy disk at the image plane. The function that describes the size of the Airy disk and the spacing between the diffraction rings in the image plane is known as the lateral point spread function (latPSF). The function that describes the size of the airy disk and the spacing between the diffraction rings in the axial direction perpendicular to the image plane is known as the axial point spread function (axPSF). In the standard treatment of diffraction, the two functions are not identical. In practice, the point spread functions are determined by

measuring the full width of the object at half maximum (FWHM) intensity in the lateral and axial directions.

Resolution is the ability to distinguish two nearby objects or two adjacent points in the same object. The Rayleigh criterion [1], which is used as a measure of resolution, states that two points can be resolved if the distance between them is greater than the distance between the center of the Airy disk formed by one object point and the first minimum in the Airy disk formed by the other object point. Cole et al. [4] characterize the resolution of the confocal microscope with the following equations:

$$\text{latPSF} = \text{Lateral resolution} = \frac{0.51 \lambda_{exc}}{NA} \quad (1)$$

$$\text{axPSF} = \text{Axial resolution} = \frac{0.88 \lambda_{exc}}{n - \sqrt{n^2 - NA^2}} \quad (2)$$

where λ_{exc} is the wavelength of the excitation light, NA is the numerical aperture of the objective lens, and n is the refractive index of the immersion medium. In both the lateral and axial cases, the resolution is measured by the full width of the prolate ellipsoids at half maximum (FWHM). Eqns. (1) and (2) are the standard equations given by Wilhelm et al. [6], and writing in a paper aimed at determining the quality of a microscope, Cole et al. [5] consider the standard equations, which predict and describe experimental results with an accuracy of 10-40%, to be appropriate estimators of the image resolution in any confocal laser scanning and wide-field microscopes as well as being “*relatively straightforward to understand and calculate.*”

Although the above equations are typically used, we have never seen a derivation of them. On the other hand, Wayne [4] has derived the resolution equations from first principles based on the electromagnetic properties of the binary photon. These derivations are consistent with the assumptions of the Kirchhoff diffraction equation. Employing Rayleigh’s criterion, the resolution equations based on the binary photon are:

$$\text{latPSF} = \text{Lateral resolution} = \frac{0.61 \lambda_{em}}{NA} \quad (3)$$

$$\text{axPSF} = \text{Axial resolution} = \frac{0.61 \pi n \lambda_{em}}{NA^2} \quad (4)$$

Both of these lateral and axial resolution equations are homogenous as they are derived using the same first-order Bessel function of the first kind as opposed to two Bessel functions of different orders. The use of identical Bessel functions is an indication that the diffraction mechanism is the same in the lateral and axial directions. Using these derivations,

the axial resolution is related to the lateral resolution by the following equation (Eqn. (77) in [4]):

$$\text{Axial resolution} = \text{Lateral resolution} \left[\frac{\pi n}{NA} \right] \quad (5)$$

where π is the ratio between the distance the binary photon propagates along the axis of propagation in one cycle and the maximum width of the binary photon, and $\frac{n}{NA}$ characterizes the optical system. Thus the mechanism of diffraction is the same in the lateral and axial directions, but the shape of the binary photon and the properties of the optical system affect the positions of the diffracted binary photons. Eqn. (5) is almost identical to the formula given by Inoué [7], based on the derivation for plane waves by Linfoot and Wolf [8] for an f/3.5 lens ($NA = 0.14$) using Lommel's sinc approximation for axial diffraction [9]:

$$\text{Axial resolution} = \text{Lateral resolution} \left[\frac{3.28n}{NA} \right] \quad (6)$$

Note that Eqn. (6), which replaces the $\pi = 3.14$ in Eqn. (5) with 3.28, while numerically close, does not rigorously apply to electromagnetic light waves that do not fulfill the assumptions of the Kirchhoff diffraction equation. By contrast, Eqn. (5), which is based on the model of the binary photon, does fulfill these assumptions. Eqn. (6) utilizes two different functions to describe resolution—a first-order Bessel function of the first kind to describe the lateral resolution and the sinc function, which is equivalent to a zeroth-order spherical Bessel function of the first kind, to describe the axial resolution.

The binary photon [10] is not an elementary particle like the quantum mechanical photon [11] but a complex entity composed of two semiphotons that rotate and oscillate within the three-dimensional space of the propagating binary photon. The movements satisfy the Schrödinger equation for bosons and the classical equations of mechanics [12] as they generate electric and magnetic fields that are orthogonal to each other and out-of-phase by a quarter of a wavelength and satisfy Faraday's law and the Ampere-Maxwell law [13]. The binary photon is an oblate spheroid in shape and has a maximal major intrinsic wavelength-dependent diameter of $\frac{\lambda}{\pi}$ perpendicular to the axis of propagation and a maximal minor intrinsic wavelength-dependent diameter of $\frac{\lambda}{\pi^2}$ along the axis of propagation [14]. The center of gravity of the binary photon propagates across a maximal distance of one contingent wavelength in one cycle [14]. Thus there is an asymmetry in the binary photon throughout one cycle, and in one cycle, the asymmetry is

characterized by the ratio of the maximal diameter to the propagation length, which is equal to $\frac{1}{\pi}$. This contrasts with the quantum mechanical photon, which is typically considered to be a spherically symmetrical zero-dimensional geometrical point traveling kinematically with a vacuum velocity c , angular momentum $\frac{h}{2\pi}$, and characterized as having energy (E) given by its frequency (ν) and linear momentum (p) given by its wavelength (λ) such that $E = h\nu$ and $p = \frac{h}{\lambda}$. The binary photon has the same energy, linear momentum, and angular momentum as the quantum mechanical photon. While the quantum mechanical photon fundamentally lacks *anschaulichkeit*, picturability, or visualizability [11], these mechanical quantities are visualizable in the binary photon [10].

Here we show that the resolution equations based on the model of the binary photon are better than the standard equations used in confocal microscopy in describing and predicting the point spread functions used to interpret images obtained with a confocal microscope. These experimental observations support the claim that binary photons may be the fundamental and irreducible component of light. Further experimental evidence in support of the fundamental nature of the binary photon has been provided recently by observations of diffraction in a refracting medium [14], where it was shown that light has both an intrinsic and a contingent wavelength that is possible for a three-dimensional object but not a mathematical point; and by observations of the Faraday effect where a magnetic field induces a rotation of the azimuth of polarized light [15], which is only possible if light has magnetic properties that requires light to be composed of at least two points and have extension in at least one-dimension giving a north-south polarity.

2. Materials and Methods

Preparation of fluorescent microspheres. We used Gold Seal (22 x 22 mm; No. 1½) cover glasses (Cat. No. 3406; Clay Adams; Becton, Dickinson and Co., Lincoln Park, NJ, USA). We selected the 0.17 mm thick cover glasses from the package using a Leitz cover glass gauge. We vortexed each stock suspension of microspheres to suspend the microspheres and then we put 7.5 μl of stock suspension of one color of PS-Speck Microscope Point Source microspheres (Cat. No. P-7220; Molecular Probes, Inc., Eugene, OR, USA) diameter $0.175 \pm 0.005 \mu\text{m}$) on one side of the whole ethanol-cleaned cover glass. The fluorescent microspheres that we initially used were a gift from Carol Bayles

of the Imaging Facility at Institute of Biotechnology at Cornell University. The solution on each cover glass was allowed to air dry for one hour under a plastic Petri plate cover to protect them from dust. The cover glass was placed bead side down on approximately 8 μ l of Invitrogen mounting medium on an ethanol-cleaned 3 \times 1 inch (0.97 to 1.07 mm thick) Gold Seal Micro Slide (Cat. No. 3010; Clay Adams; Becton, Dickinson and Co., Lincoln Park, NJ, USA). We pushed down on the cover glass with a cotton swab to spread the viscous mounting medium. After ten minutes, each cover glass was ringed with two thin layers of clear Diamond Shine nail polish (Sally Hansen, New York, NY, USA) to make the slides permanent. The slides were stored at 4 C in the dark. On one occasion, the acetone in the nail polish must have seeped under the coverslip because the fluorescent microspheres were suspended in a fluorescent background. The nail polish around the edges of the coverslip appeared white as opposed to clear. This slide was discarded.

The excitation/emission wavelengths of the yellow-green microspheres were 505 nm/515 nm.

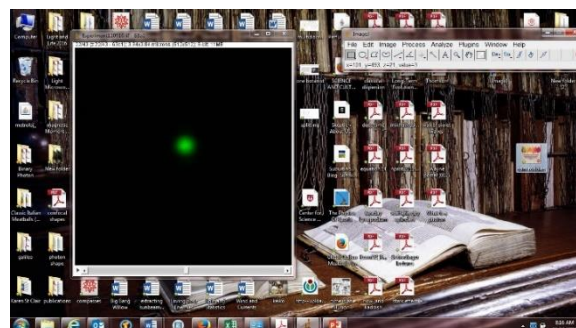
We observed the microspheres at the Boyce Thompson Institute Plant Cell Imaging Center with a Leica TCS SP5 Laser Scanning Confocal Microscope (Leica Microsystems Exton, PA USA) equipped with a 100 \times (NA 1.44) oil immersion objective, a 63 \times (NA 1.40) oil immersion objective, a 63 \times (NA 1.20) water immersion objective, a 40 \times (NA 1.25) oil immersion objective, and a 40 \times (NA 0.85) dry objective (<https://btscience.org/our-research/research-facilities/plant-cell-imaging-center/pcic-microscopes/>). All the objectives were HCX infinity-corrected Plan Apochromats. The pinhole was set at 1 Abbe unit. The fluorescent microspheres were excited with the blue argon ion laser (496 nm), and emitted light was collected between 510 nm and 551 nm. Z stacks composed of 60–109 8-bit images (512 \times 512) were collected with a frame speed of 2.6 frames/second using 400 Hz scanner speed. The step size was 0.04 μ m in the image space. The time necessary to acquire a Z stack varied from 155 to 284 seconds. When observing single microspheres in a field, the initial laser power was reduced to 10% for the 100 \times (NA 1.44) oil immersion objective, the 63 \times (NA 1.40) oil immersion objective, and the 63 \times (NA 1.20) water immersion objective; to 14% for the 40 \times (NA 1.25) oil immersion objective, and to 25% for the 40 \times (NA 0.85) dry objective. The immersion oil was Leica Type F ($n_{23} = 1.5180$).

We initially used the MetroloJ plugin (<https://imagejdocu.tudor.lu/plugin/analysis/metroloj/>

[start](#)) in ImageJ to measure the lateral and axial point spread functions. Then we used the Leica software. The MetroloJ results were consistently and significantly smaller than the Leica results. This led us to develop our own method using ImageJ. The results using the Leica software and our custom method using ImageJ were consistent. The point spread function was measured using the Leica LAS AF v.2.6.0 software and custom software in ImageJ

Custom procedure for the Analysis of FWHM:

Open .lif file with ImageJ (Note that stack will be black because it starts at first slice that does not



include the spot; Fig. 1).

Fig. 1: Image of the .lif file of a fluorescent microsphere (l) and the ImageJ toolbar (r).

Click on Image/Stacks/Orthogonal Views. Then move cross hairs until the XY, YZ, and XZ images are optimally bright and symmetrical (Fig. 2). Then



save the three images as .tif files.

Fig. 2: The crosshairs are placed so that the XY (l), YZ (c), and XY (r) images are maximally bright and symmetrical.

Open the XZ image file. Put the rectangular ROI around the whole image. Click on Analyze/Plot Profile. Click on Data/Copy 1st Data Set. Click on Analyze/Tools/Curve Fitting. Replace any numerical data in box with data from the image using the Paste

command. Choose Gaussian (where it says “straight line”). Click on Fit. Record the standard deviation (d).

The Gaussian curve fitting program in ImageJ relates the intensity of a pixel (y) to the position (x) of the pixel along the crosshair using the following equation and solves for the parameters (a, b, c, and d):

$$y = a + (b - a)e^{-\left(\frac{x-c}{d}\right)^2} \quad (7)$$

Calculate FWHM for axial resolution using the following formula:

$$\text{FWHM (nm)} = d * 2.3548 * 1000 \quad (8)$$

where 2.3548 is equal to $2\sqrt{2 \ln 2}$ and the 1000 is the conversion factor between μm and nm (Fig. 3). Repeat for images of the XY and YZ planes. Present data as $\bar{x} \pm \text{S.D.}$

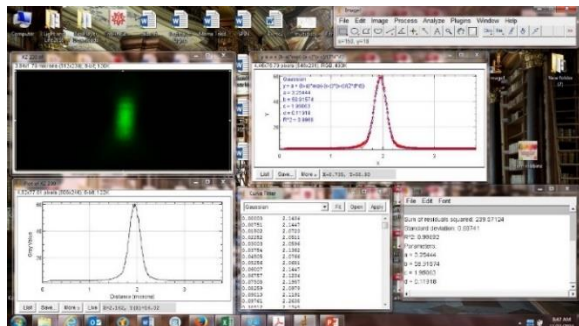


Fig. 3: The XZ image (top left), the intensity profile (bottom left), the Gaussian fit (top right), the list of data for a Gaussian fit (bottom, center), and the results of the Gaussian fit (bottom right).

3. Results and Discussion

Images of each fluorescent microsphere were observed in the XY plane, the YZ plane, and the XZ plane. (Fig. 4). Each of the 51 microspheres observed appeared to be a prolate ellipsoid relative to the optical axis of the microscope. Images were taken with a variety of objective lenses.

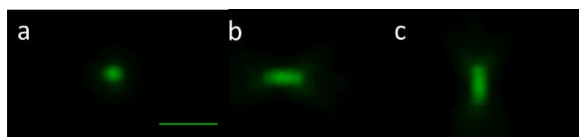


Fig. 4: Maximal projection images of a 175 nm in diameter microsphere created by a confocal laser scanning microscope using a $63\times$ (NA 1.44) oil-immersion objective lens. (a) XY plane, (b) YZ plane, and (c) XZ plane. Scale bar = $1 \mu\text{m}$.

The FWHM of the images of the fluorescent microspheres were determined using the Leica software and the custom ImageJ software. The FWHM of the image in the XY plane and the minor axes (X and Y) in the images in the YZ and XZ planes were used to determine the lateral PSF and the lateral resolution. The FWHM of the major axis in the images in the YZ and XZ planes were used to determine the axial PSF and the axial resolution. The average values of the Leica measurements and the ImageJ measurements are plotted separately and the average of the two techniques are also plotted (Fig. 5). The resolution equations based on the model of the binary photon (Eqns. (3) and (4)) are more accurate estimators of the observed lateral and axial resolution compared with the standard equations (Eqns. (1) and (2)).

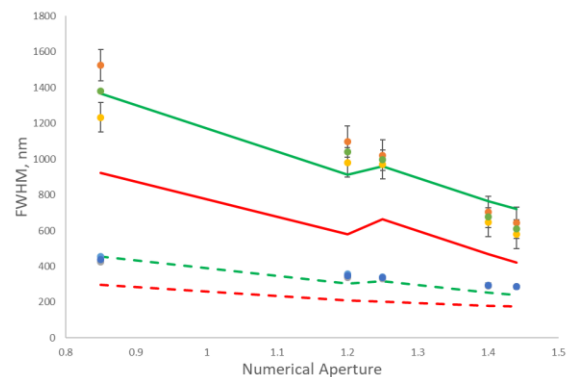


Fig. 5. Observations: Lateral FWHM (Leica ●; ImageJ ●; Average of two techniques ●); Axial FWHM (Leica ●; ImageJ ●; Average of two techniques ●); Theoretical: Eqn. (1) - -; Eqn. (2) - -; Eqn. (3) - -; Eqn. (4) - -.

The accuracy of the equations (3 and 4) derived on the basis of the model of the binary photon [4] are better than the accuracy of the standard equations (1 and 2) used in confocal microscopy [5,6] in predicting the lateral and axial FWHM of the 175 nm in diameter fluorescent microspheres observed with a confocal microscope. This suggests that the asymmetry in the inflation of the image is not due only to the limits of the optical system but to the shape of the binary photon. Therefore, not only are the equations based on the binary photon useful for quantifying images taken with a microscope, but the accuracy of the equations based on the binary photon indicate that the binary photons, which satisfy Schrödinger’s equation for a boson, obey Faraday’s law and the Ampere-Maxwell law, and fulfill the assumptions of Kirchhoff’s diffraction equation, may be the fundamental and irreducible component of light [4,12,13,16].

References

- [1] R. Wayne, *Light and Video Microscopy*, Third edition (Elsevier, Amsterdam, 2019).
- [2] S. Inoué, *Video Microscopy* (Plenum Press, New York, 1986).
- [3] H. E. Keller, Objective lenses for confocal microscopy, pp. 111-126. In: *Handbook of Biological Confocal Microscopy*. Second edition, J. B. Pawley, ed. (Springer Science + Business Media, New York, 1995).
- [4] R. Wayne, *The Kirchhoff diffraction equation based on the electromagnetic properties of the binary photon*. African Review of Physics submitted.
- [5] R. W. Cole, T. Jinadas, and C. M. Brown, Nature Protocols **6**, 1929 (2011).
- [6] S. Wilhelm, B. Gröbler, M. Gluch, and H. Heinz, *Principles: Confocal Laser Scanning Microscopy* (Carl Zeiss, Jena, 1997).
- [7] S. Inoué, Foundations of confocal scanned imaging in light microscopy, pp. 1-17. In: *Handbook of Biological Confocal Microscopy*. Second edition, J. B. Pawley, ed. (Springer Science + Business Media, New York, 1995).
- [8] E. H. Linfoot and E. Wolf, Proc. Phys. Soc. B **69**, 823 (1956).
- [9] E. Lommel, Die Beugungserscheinungen einer kreisrunden Oeffnung und eines kreisrunden Schirmchens: theoretisch und experimentel. Abhandlungen der mathematisch-physikalischen Classe der Königlich Bayerischen Akademie der Wissenschaften **XV** (II), 229 (1885).
- [10] R. Wayne, *The Binary Photon: A heuristic proposal to address the enigmatic properties of light*. African Review of Physics submitted.
- [11] K. Hentschel, *Photons: The History and Mental Models of Light Quanta* (Springer, Cham, Switzerland, 2018).
- [12] R. Wayne, *Using the Schrödinger equation for a boson to relate the wave-like qualities and quantized particle-like quantities of the binary photon in Euclidean space and Newtonian time*. African Review of Physics submitted.
- [13] R. Wayne, African Review of Physics **13**, 128 (2018).
- [14] M. Halberg, M. Rutzke, and R. Wayne, *The intrinsic and contingent properties of the binary photon: The equivalence of color, wavelength, and frequency in dielectric media*. African Review of Physics submitted.
- [15] C. Faraday, R. Furnas, M. Rutzke, and R. Wayne, *The action of a magnetic field on light and matter: Possible direct interaction between magnetism and light*. African Review of Physics submitted.
- [16] R. Wayne, Nature of Light from the Perspective of a Biologist: What is a Photon? In: *Handbook of Photosynthesis*. Third edition, M. Pessaraki, ed. (CRC Press, Taylor and Francis Group, London, 2015).

Received: 06 June, 2020

Accepted: 18 February, 2021